

# TUSC5 regulates insulin-mediated adipose tissue glucose uptake by modulation of GLUT4 recycling



Nigel Beaton<sup>1</sup>, Carla Rudigier<sup>1</sup>, Hansjörg Moest<sup>1</sup>, Sebastian Müller<sup>1</sup>, Nadja Mrosek<sup>1</sup>, Eva Röder<sup>1</sup>, Gottfried Rudofsky<sup>2</sup>, Thomas Rüllicke<sup>3</sup>, Jozef Ukropec<sup>4</sup>, Barbara Ukropcova<sup>4,5</sup>, Robert Augustin<sup>6,7</sup>, Heike Neubauer<sup>6</sup>, Christian Wolfrum<sup>1,\*</sup>

## ABSTRACT

**Objective:** Failure to properly dispose of glucose in response to insulin is a serious health problem, occurring during obesity and is associated with type 2 diabetes development. Insulin-stimulated glucose uptake is facilitated by the translocation and plasma membrane fusion of vesicles containing glucose transporter 4 (GLUT4), the rate-limiting step of post-prandial glucose disposal.

**Methods:** We analyzed the role of Tusc5 in the regulation of insulin-stimulated Glut4-mediated glucose uptake *in vitro* and *in vivo*. Furthermore, we measured Tusc5 expression in two patient cohorts.

**Results:** Herein, we report that TUSC5 controls insulin-stimulated glucose uptake in adipocytes, *in vitro* and *in vivo*. TUSC5 facilitates the proper recycling of GLUT4 and other key trafficking proteins during prolonged insulin stimulation, thereby enabling proper protein localization and complete vesicle formation, processes that ultimately enable insulin-stimulated glucose uptake. *Tusc5* knockout mice exhibit impaired glucose disposal and TUSC5 expression is predictive of glucose tolerance in obese individuals, independent of body weight. Furthermore, we show that TUSC5 is a PPAR $\gamma$  target and in its absence the anti-diabetic effects of TZDs are significantly blunted.

**Conclusions:** Collectively, these findings establish TUSC5 as an adipose tissue-specific protein that enables proper protein recycling, linking the ubiquitous vesicle traffic machinery with tissue-specific insulin-mediated glucose uptake into adipose tissue and the maintenance of a healthy metabolic phenotype in mice and humans.

© 2015 The Authors. Published by Elsevier GmbH. This is an open access article under the CC BY-NC-ND license (<http://creativecommons.org/licenses/by-nc-nd/4.0/>).

**Keywords** Obesity; Glucose uptake; Type 2 diabetes; Insulin resistance

## 1. INTRODUCTION

In healthy individuals post-prandial glucose is quickly cleared from the circulation into muscle and adipose tissue in response to insulin stimulation by ATP-independent facilitative diffusion through glucose transporter 4 (GLUT4) [1]. During insulin resistance, a common comorbidity of obesity and a hallmark of type 2 diabetes, GLUT4 translocation to the plasma membrane is impaired [2,3]. In both muscle and adipocyte-specific GLUT4 knockout mice, glucose homeostasis is impaired and insulin resistance develops [4,5]. These same diabetic symptoms are also present in heterozygous GLUT4 mice, despite the fact that these mice do not become obese [6]. In accordance, global and tissue-specific GLUT4 over-expression mouse models exhibit improved insulin sensitivity and glucose homeostasis, even in obese and diabetic mice [7–10]. Collectively, these findings demonstrate GLUT4's importance in the maintenance of a healthy metabolic phenotype.

Functional regulation of GLUT4 is accomplished via control of its cellular trafficking, a process that is driven by a variety of proteins [11–13]. These proteins ensure proper vesicle fusion (e.g. VAMPs) [14,15], confer vesicle motility and directionality (e.g. Rabs, IRAP) [11,16], participate in protein recycling (e.g. STX6) [17,18] and act as vesicle tethers (e.g. TUG) [19,20]. Several of these proteins co-localize with GLUT4 to specialized vesicles termed GLUT4 storage vesicles (GSVs) [21,22] that act as the main intracellular insulin-responsive GLUT4 reservoir [23]. Interestingly, each of the proteins with a known role in GLUT4 trafficking also participates in similar vesicle traffic systems in other tissues [24–26]; currently no adipose tissue-specific protein link exists between the specific insulin-mediated function of GLUT4 and the ubiquitous trafficking machinery it exploits [22].

Protein recycling is a particularly vital step to the long-term function of GLUT4 [27]. GLUT4 is cleared from the plasma membrane by endocytosis after the cessation of insulin stimulation or during a prolonged

<sup>1</sup>Institute of Food, Nutrition and Health, ETH Zurich, Schwerzenbach, Switzerland <sup>2</sup>Department of Medicine I and Clinical Chemistry, University of Heidelberg, Heidelberg, Germany <sup>3</sup>Institute of Laboratory Animal Science, Vetmeduni, Vienna, Austria <sup>4</sup>Institute of Experimental Endocrinology, Slovak Academy of Sciences, Bratislava, Slovakia <sup>5</sup>Institute of Pathophysiology, School of Medicine, Comenius University, Bratislava, Slovakia <sup>6</sup>CardioMetabolic Diseases Research, Boehringer Ingelheim Pharma GmbH&Co. KG, Biberach a.d. Riss, Germany <sup>7</sup>Translational Medicine and Clinical Pharmacology, Boehringer Ingelheim Pharma GmbH&CoKG, Biberach a.d. Riss, Germany

\*Corresponding author. ETH Zürich, Schorenstrasse 16, CH-8603 Schwerzenbach, Switzerland. Tel.: +41 44 6557451. E-mail: [christian-wolfrum@ethz.ch](mailto:christian-wolfrum@ethz.ch) (C. Wolfrum).

Received August 6, 2015 • Revision received August 11, 2015 • Accepted August 18, 2015 • Available online 28 August 2015

<http://dx.doi.org/10.1016/j.molmet.2015.08.003>

insulin stimulus [28–31]. Following internalization, GLUT4 is enriched in endosomal compartments containing proteins that actively participate in protein recycling, such as syntaxins 6 and 16 [17,18] and VAMP3 [32], and cargo proteins, such as the transferrin receptor (TfR) [33,34]. It is through this endosomal recycling pathway that GLUT4 is either shuttled back to the plasma membrane, in the case of prolonged insulin stimulation, or, if insulin stimulation has ceased, sequestered back in GSVs [11,12,35–37].

Tumor suppressor candidate 5 (TUSC5), is a protein abundantly expressed in white [38] and brown adipose tissue [39] and Tusc5 mRNA expression increases during adipogenesis [39,40]. Evidence exists that TUSC5 is a PPAR $\gamma$  target gene as PPAR $\gamma$  has been shown to bind to the promoter region of TUSC5 [41] and Tusc5 mRNA expression increases in adipocytes treated with the PPAR $\gamma$  agonist GW1929 [40]. Although these data collectively suggest that TUSC5 may serve a function in mature adipocytes, to date, the mechanism of action, physiological consequences and the importance of TUSC5 in the pathogenesis of obesity remain unknown.

## 2. MATERIAL AND METHODS

### 2.1. Materials

All chemicals were purchased from Sigma–Aldrich unless specified otherwise.

### 2.2. Animals

C57Bl/6 mice were housed in a pathogen-free animal facility on a 12-h/12-h light/dark cycle with free access to food and water.

### 2.3. Plasmids

For lentivirus production Mission shRNA (Sigma–Aldrich) against TUSC5 was used. For adenovirus production shRNAs against TUSC5 were designed (<http://maidesigner.invitrogen.com/rnaiexpress/>), cloned into pENTR-U6 and recombined into pAd-BLOCK-iT-DEST (Invitrogen). VAMP2 cDNA amplified from murine adipocyte cDNA was cloned into pCDNA3.1/V5-His. Primer/shRNA sequences are available upon request.

### 2.4. Western blot analysis

Whole cell lysates were prepared as previously described [42]. For western blot analysis (and other experiments) the following antibodies were used: TUSC5 (Santa Cruz Biotechnology, SC-292062, 1:1000), GLUT4 (Cell Signaling, #2213, 1:1000; Millipore, 07-1404, 1:1000), Akt (Cell Signaling, #9272, 1:1000), phospho-Akt (Cell Signaling, #4056, 1:1000), Sortilin (BD Bioscience, #612100, 1:1000), V5 (Invitrogen, #46-07-05, 1:5000), Cellugyrin (Santa Cruz Biotechnology, SC-68935), c-Myc (Sigma Aldrich, C3956) and  $\gamma$ Tubulin (Sigma–Aldrich, T6557, 1:6000). Western blot quantification was done using ImageJ software.

### 2.5. Cell culture

3T3-L1 cells and immortalized brown preadipocytes were seeded onto collagen-coated plates and grown in high-glucose DMEM supplemented with 10% fetal bovine serum (FBS) and 1% penicillin/streptomycin (all Invitrogen) prior to differentiation. Three days post-confluent 3T3-L1 cells were treated with induction cocktail (1  $\mu$ g/ml insulin, 1  $\mu$ M dexamethasone and 115  $\mu$ g/ml isobutyl-methylxanthine) for 2 days followed by insulin media (1  $\mu$ g/ml insulin) for 2 days and DMEM for 3 days. For rosiglitazone treatment cells were stimulated with 1  $\mu$ M rosiglitazone in DMEM and media was changed every 24 h. Immortalized brown preadipocytes were induced at day of confluence

with 117 ng/ml insulin, 1  $\mu$ M dexamethasone, 115  $\mu$ g/ml isobutyl-methylxanthine, 125  $\mu$ M indomethacin, 1 nM Rosiglitazone and 1 nM T3 for 2 days and subsequently maintained in insulin (117 ng/ml)/T3 (1 nM) media for differentiation into mature adipocytes. L6 and L6-Glut4myc cells were obtained from the Klip lab (The Hospital for Sick Children, Toronto, CA) and cultured in low glucose  $\alpha$ -MEM (Invitrogen) enriched with 10% FBS and 1% penicillin/streptomycin. Formation of myotubes was stimulated by decreasing the FBS concentration to 2% for the entire duration of differentiation.

### 2.6. Real-time PCR

mRNA was isolated and transcribed into cDNA using the Multi-MACS cDNA kit (Miltenyi). Expression levels of mRNA were assessed by real-time PCR using SybrGreen (Invitrogen) according to the manufacturer's protocol. Expression was normalized to GAPDH or 36B4. Primer sequences are available upon request.

### 2.7. Viral infection

Lentiviral stocks were prepared as previously described [42]. For lipid droplet assays 3T3-L1 cells were infected for 24 h with virus containing media supplemented with polybrene (8  $\mu$ g/ml) 3 days before adipogenic induction. Adenovirus production was done in HEK293A cells with pAd-TUSC5-shRNA crude lysate. Adenovirus was purified using a column system (Virapur). For mature adipocyte experiments, adenoviral infection was done 2 days after 3T3-L1 adipogenic induction or at d8 of differentiation in Opti-MEM media (Invitrogen) supplemented with 1.2% poly-lysine for 24 h. All mature adipocyte experiments were performed 5–6 days after adenovirus infection. Likewise, L6 and L6-Glut4myc cells were virus infected at d3 of differentiation and experiments performed at d8.

### 2.8. Epididymal fat pad injections

Adenovirus was injected (40  $\mu$ l,  $1 \times 10^{10}$  PFU/ml per fat pad) into the epididymal fat pad of ten-weeks old C57Bl/6 mice [43]. To place the injections exclusively into the epididymal fat pad, anaesthetized mice were fixed in a dorsal position and the pads were exposed under sterile conditions. After midline laparotomy (incision length 0.5–1 cm ending approximately 1 cm rostral to the urethral orifice), both fat pads were carefully pulled out of the intra-abdominal perigonadal area. Adenovirus was slowly injected with a 30G needle (BD Diabetes), which penetrated the distal end of the depot first and was then pushed forward to the proximal end. After careful repositioning of the intra-abdominal perigonadal area, the abdominal wall was sutured in two layers (the peritoneum parietale, followed by the skin) with 2–3 single stitches of absorbable suturing material (Vicryl 6-0, Ethicon). Anaesthesia was performed by isoflurane (induction: 4–5%, maintenance: 1–3%) and for analgesia Meloxicam (5 mg/kg, sc) was administered 30 min prior to surgery and post-operatively via drinking water (1.7  $\mu$ g/ml) for 3–4 days. Six days after injection the mice were fasted for 16 h prior to experiments.

### 2.9. Glucose uptake

*In vitro* glucose uptake was performed on 3T3-L1 adipocytes 5 days after adenoviral knockdown of TUSC5. Briefly, cells were incubated at 37  $^{\circ}$ C in Krebs–Ringer buffer containing insulin, 2 mM glucose and  $^{14}$ C-deoxyglucose (200 cpm/ml). After 2 h cells were washed twice with ice cold PBS and lysed by one freeze thaw cycle in 2 M NaOH. Lysates were mixed with 3 ml scintillation cocktail and intracellular radioactivity was quantified in disintegrations per minute (dpm).

*In vivo* glucose uptake was performed in C57Bl/6 mice six days after adenoviral injection into epididymal adipose tissue. In short, mice were

fasted overnight (16 h) prior to receiving a tail vein injection of 100  $\mu$ l  $^{14}$ C-deoxyglucose (250,000 cpm/ $\mu$ l) and 0.3  $\mu$ l  $^3$ H-mannitol (2,600,000 cpm/ $\mu$ l) with insulin (0.5 IU/kg) or 0.9% NaCl solution. Mice were sacrificed by cervical dislocation after 30 min and eWAT depots were removed, weighed and dissolved for 1 h in 1 M NaOH at 60 °C. To calculate 2-deoxyglucose-6-phosphate synthesis lysate was neutralized with an equal volume of 1 M HCl.  $^{14}$ C-deoxyglucose was isolated from lysates by mixing 200  $\mu$ l of lysate with 500  $\mu$ l of 0.3 M ZnSO<sub>4</sub> and 500  $\mu$ l of 0.3 M Ba(OH)<sub>2</sub>. A  $^{14}$ C-deoxyglucose and  $^{14}$ C-deoxyglucose-6-phosphate mix was isolated by mixing 200  $\mu$ l lysate with 1 ml of 6% perchloric acid. Both samples were vortexed and centrifuged for 2 min and 13,000g. 800  $\mu$ l of each supernatant was mixed with 3 ml scintillation cocktail total radioactivity was quantified in dpm and 2-deoxyglucose-6-phosphate was calculated.

### 2.10. Adipocyte differentiation analysis

Differentiated cells were fixed with 4% formaldehyde prior to staining with Hoechst (nuclei), BODIPY (lipid droplets) and Syto60 (cytosol) (Invitrogen). Sixteen pictures were taken per well with an automatic imaging system (Operetta) and analyzed for lipid droplet sizes using Cell Profiler software [42,43].

### 2.11. Tissue whole mount staining

Prior to eWAT isolation C57Bl/6 mice were perfused with 0.9% NaCl solution. eWAT was isolated and cut into 2–4 mm pieces and fixed with 4% paraformaldehyde. Tissue sections were permeabilized with PBS-T (PBS with 0.5% Triton-X) followed by blocking for 2 h in blocking buffer (PBS, 5% donkey serum, 0.05% sodium azide, 1% BSA, 0.1% Triton-X) and overnight incubation at 4 °C with primary antibodies (TUSC5, GLUT4, 1:750). The following day sections were washed (4 times, 20 min) with PBS-T and incubated at room temperature with secondary antibody ( $\alpha$ -rabbit Alexa488, A21206, Invitrogen;  $\alpha$ -mouse Alexa 568, A11031, Invitrogen; both 1:300) for 2 h. Sections were washed (4 times, 20 min each) with PBS-T and mounted with Vectashield (Reactolab) prior to confocal imaging (Leica SP2-AOBS).

### 2.12. Immunofluorescence

Insulin-stimulated Glut4/Vamp3 localization was visualized as previously described [44]. Briefly, mature (d12) 3T3-L1 adipocytes were fasted in serum free DMEM for three hours and stimulated with 100 nM insulin (for indicated times) and washed (all washes were 6 times, 5 min, PBS). Cells were then fixed and permeabilized (4% formaldehyde, 0.18% triton) for 10 min, washed and blocked (PBS, 1% BSA, 5% FBS) for 1 h. After washing, cells were incubated with primary antibody (TUSC5, GLUT4 (Santa Cruz c-20, #sc-1608) or VAMP3 (Novus Biologicals, #NB300-510); all 1:300) in blocking buffer for 1 h at RT. Cells were washed and incubated with secondary antibody ( $\alpha$ -rabbit Alexa488, A21206, Invitrogen;  $\alpha$ -mouse Alexa 568, A11031, Invitrogen; both 1:750) in blocking buffer for 1 h at room temperature. Finally, cells were washed and mounted in Vectashield with DAPI for confocal imaging (Leica SP5 Mid-UV/Vis). Quantification of Glut4/Vamp3 distribution was done with Cell profiler.

### 2.13. Immunoprecipitations

All immunoprecipitations were performed from differentiated 3T3-L1 cells. Lysis was done in RIPA buffer (1% NP40, 2% (v/v) protease inhibitors (Roche), pH 7.5). Briefly, cell lysate was incubated overnight at 4 °C on an overhead rotator with 5  $\mu$ g of antibody. Next, 60  $\mu$ l of Protein G-PLUS Agarose (Santa Cruz) (pre-washed twice with RIPA buffer minus NP40) was incubated with lysate for 2 h at 4 °C on

overhead rotator. Agarose beads were washed 5 times (RIPA minus NP40, 1000 g spin for 2 min between washes) and proteins were eluted in supernatant for western blots in 100  $\mu$ l of 2 $\times$  Laemmli buffer (boiled for 10 min before a brief full speed spin to pellet the remaining agarose). For mass spectrometry, agarose beads were transferred to Bio-Spin columns (Bio Rad, #732-6204) for final three RIPA washes, then to new columns for 2 additional washes with 50 mM ammonium bicarbonate buffer. Proteins were digested overnight at 37 °C with 0.5  $\mu$ g trypsin in ammonium bicarbonate buffer and peptide elution was collected and frozen.

### 2.14. Mass spectrometry

After peptide elution, samples were reduced and alkylated with 5 mM TCEP (tris(2-carboxyethyl)phosphine) and 10 mM Iodoacetamide. Peptides were cleaned with 3–30  $\mu$ g UltraMicroSpin columns (The Nest Group), dried in a speed-vac and resolubilized in 0.1% formic acid.

For reversed-phase chromatography, a high-performance liquid chromatography (HPLC) column (75- $\mu$ m inner diameter, New Objective) that was packed in-house with a 10-cm stationary phase (Magic C18AQ, 200 E, 3  $\mu$ m, Michrom Bioresources) was used which was connected to either a nano-flow HPLC (nanoLC-Ultra 1D plus, Eksigent) and an autosampler (nanoLC AS-2, Eksigent) or a *Proxeon* easy-nLC system (Odense, Denmark). The HPLC was coupled via a nano-electrospray ion source (Thermo Scientific) to a LTQ-Orbitrap XL mass spectrometer (Thermo Scientific). After loading the peptides on the column with 95% buffer A (98% H<sub>2</sub>O, 2% acetonitrile, 0.1% formic acid), they were eluted at flow rate of 300 nl/min over a 60 min linear gradient from 5 to 35% buffer B (2% H<sub>2</sub>O, 98% acetonitrile, 0.1% formic acid). Mass spectra were acquired in a data-dependent acquisition mode with one cycle consisting of one MS1 scan followed by 3 or 5 MS/MS scans. Precursor ions were monitored in the mass range of 350–1650 *m/z* by a high resolution MS1 scan acquired in the Orbitrap (60,000 FWHM, target value 10<sup>6</sup>). For MS/MS scans, precursor ions were fragmented by collision induced dissociation in the ion trap (minimum signal threshold 150, target value 10<sup>4</sup>, isolation width 2 *m/z*). Unassigned charged states, as well as singly charged ions, were excluded from fragmentation and the dynamic exclusion was set to 10 s.

ReadW (version 4.3.1) was used to convert raw data into the open mzXML format. The mzXML files were searched with SORCERER (Version 3.5) against the mouse UniProtKB/Swiss-Prot protein databases (release 2012\_07). Search parameters for peptide-spectrum matching contained a peptide mass tolerance of 50 ppm, a minimum of one tryptic terminus, a maximum of one internal trypsin cleavage sites and cysteine carbamidomethylation (+57.021 Da) as a static amino acid modification. For probability scoring of peptides and proteins the Trans-Proteomic Pipeline (Version 4.0.2) was used including PeptideProphet and ProteinProphet, and protein identifications were filtered to a false-discovery rate of  $\leq$ 1%. For MS1 based label-free quantification of the identified peptides, MS1 ions signals corresponding to peptide features were extracted with the SuperHirn (Version 03) software. After intensity normalization, peptide signal intensities belonging to the same protein were summarized followed by statistical analysis of the data.

### 2.15. Cell fractionation assays

Fractionation of 3T3-L1 adipocytes or primary adipose tissue into plasma membrane and low-density microsome (LDM) fractions was performed as previously described [45]. For further LDM fractionation the fraction was resuspended in 50  $\mu$ l TES buffer and layered on top of

phosphate buffer (16 mM Na<sub>2</sub>HPO<sub>4</sub>, 4 mM NaH<sub>2</sub>PO<sub>4</sub>, 50% sucrose (w/v)) and centrifuged at 150,000g for 30 min. Fractions were collected in 100 µl aliquots.

#### 2.16. Plasma membrane lawn assay

Differentiated 3T3-L1 cells (Lab-Tek chamber slides) were serum starved for 2 h prior to insulin treatment. Cells were sequentially washed in PBS, 1 mg/ml of poly-lysine in buffer A (70 mM KCl, 30 mM HEPES, 5 mM MgCl<sub>2</sub>, 3 mM EGTA, pH 7.5) for 30 s, two washes in hypotonic buffer A (1/3 buffer A, 2/3 H<sub>2</sub>O) and sonicated (amplitude = 1, 2 s) in buffer A. Lawns were washed 3 times in PBS and stained for plasma membrane with CellMask (Invitrogen) at 5 µg/ml according to manufacturer's protocol. Lawns were fixed (4% formaldehyde), blocked (5% goat serum), incubated with GLUT4 antibody (1:200, Millipore) followed by Alexa488 secondary antibody (1:300, Invitrogen). Both antibodies incubated for 1 h at room temperature. Three PBS washes were performed between steps. Lawns were mounted with Vectashield for imaging (Leica SP2-AOBS).

#### 2.17. GLUT4-myc assays

GLUT4-myc plasma membrane integration assays were done as previously described [46,47]; however, the re-warming endocytosis step was omitted. 3T3-L1 adipocytes were cultured overexpressing exofacially myc-tagged GLUT4, with or without a TUSC5 knockdown. Cells were serum-starved (2 h) and subsequently stimulated with insulin (15 min) in DMEM. All washes and treatments were done at 4 °C in PBS<sup>+</sup> (PBS, 1 mM CaCl<sub>2</sub>, 1 mM MgCl<sub>2</sub>). Non-permeabilized cells were blocked (5% goat serum, 20 min), labeled with myc antibody (Sigma—Aldrich, 1:250 in 3% goat serum, 1 h) and fixed in 4% paraformaldehyde. Excess fixative was quenched in 100 mM glycine. GLUT4-myc bound antibody was detected with HRP-conjugated secondary antibody (α-rabbit HRP, Jackson Immune Research, #111-035-144, 1:1000 in 3% goat serum, 1 h) followed by HRP detection by OPD assay as previously described [47]. Total GLUT4-myc expression was checked in permeabilized cells (0.1% Triton-X in PBS<sup>+</sup>) (Supplementary Figure 4). A modified protocol was used to assess surface Glut4myc levels in L6 and L6-Glut4myc cells overexpressing Tusc5. Insulin stimulation was terminated with cold PBS and cells subsequently fixed in 4% formaldehyde for 10 min at 4 °C. The fixative was quenched as above and cells blocked with 5% BSA in PBS for 40 min at RT. Primary (c-myc A-14, sc-789, 1:200) and secondary antibody incubations were done for 1 h at 37 °C, each followed by thoroughly washing with PBS/0.05% Tween-20 (3×) and PBS<sup>+</sup> (3×). ABTS was used as substrate for HRP, the reaction stopped with 1% SDS and the absorbance was measured at 405 nm. Cells for immunofluorescence assays were cultured on chamber slides and subjected to the same staining protocol (c-Myc antibody at 1:150, 5% goat serum) up to the fixation step. Subsequently, cells were stained with α-rabbit Alexa488 (Invitrogen, 1:300, 5% goat serum, 1 h) and mounted in Vectashield with DAPI for confocal imaging (Leica SP2-AOBS).

#### 2.18. Tusc5 knockout mice

Embryonic stem cells containing a TUSC5 targeting construct (Tusc5(tm1a(KOMP)Wtsi), EPD0757\_5\_F08) were obtained from knockout mouse project and micro-injected to generate C57Bl/6N founder mice. Germline transmission as achieved by crossing of founders against C57Bl/6N wild type mice.

#### 2.19. TZD treatment

Rosiglitazone gavages (10 mg per kg mouse) were done in 100 µl of vegetable oil on a daily basis in both wild-type and TUSC5 knockout

cohorts. Re-fed blood glucose was checked by tail vein blood 2 h into the dark cycle. Intraperitoneal glucose tolerance tests and insulin tolerance tests on HFD mice were done via intraperitoneal injection of mice with glucose (1 g per kg mouse) or insulin (1 IU per kg) after a 6 h fast. Blood glucose was checked by tail vein blood at the indicated time points.

#### 2.20. Adipose tissue collection and isolation of adipocytes

Subcutaneous adipose tissue (scWAT) samples were taken by needle biopsy from abdominal region in the fasted state as described previously [48]. Samples were immediately cleaned up from blood and connective tissue and (i) frozen in liquid nitrogen or (ii) collagenase-digested to isolate adipocytes and stromal fraction. Adipocyte's diameter was determined by analysis of multiple microscopic images (ImageJ software, UTHSCSA, USA). Average diameter of at least 100 cells from each adipocyte suspension was calculated.

#### 2.21. Euglycemic hyperinsulinemic clamp study

Insulin sensitivity was measured by the euglycemic hyperinsulinemic clamp (clamp). Examination started in the morning after an overnight fast. Patients were advised to minimize moderate/vigorous physical activity and abstain from alcohol for at least 48 h prior to the clamp. Two intravenous cannulas were inserted into the antecubital veins of both arms: the first for administration of insulin and 20% glucose with KCl and the second (contra lateral arm) for blood sampling. The hand was kept warm to "arterialize" blood samples. A primed (80 mU/m<sup>-2</sup>/min<sup>-1</sup>) continuous (40 mU/m<sup>-2</sup>/min<sup>-1</sup>) insulin (Actrapid 100 IU/ml, Novo Nordisk, Denmark) infusion was used to achieve hyperinsulinemia. Blood glucose was measured in 5-minute intervals. Euglycemia was maintained using variable infusion rate of 20% glucose. The whole body insulin sensitivity index (M-value) was calculated from the steady state plasma glucose infusion rate required to maintain euglycemia, expressed per kg body weight per minute during the last 60 min of the 2.5 h clamp.

#### 2.22. Bioethics

All animal studies were approved by the Canton of Zurich Veterinary Office. The human work on obese subjects was carried out at the University Hospital of Heidelberg, with approval from the ethics committee of the hospital. Informed consent was obtained from all patients participating in this study.

#### 2.23. Human studies ethics statement

All studies were approved by the Ethics Committee of the University Hospital Bratislava, Comenius University Bratislava and the university hospital Heidelberg and are conforming to the ethical guidelines of the 2000 Helsinki declaration. All participants provided witnessed written informed consent prior entering the study.

#### 2.24. Statistical analysis

Results are given as mean ± standard error. Statistical analyses were performed using a two-tailed Student's *t*-test. Linear regression was calculated using Graph Pad Prism.

### 3. RESULTS

#### 3.1. TUSC5 co-localizes with GLUT4 and is required for insulin-stimulated glucose uptake

We initially identified Tusc5 as a gene highly expressed in inguinal white adipose tissue (iWAT), epididymal white adipose tissue (eWAT) and brown adipose tissue (BAT) with a low degree of expression in skeletal muscle and heart (Figure 1A). As Tusc5 mRNA expression is

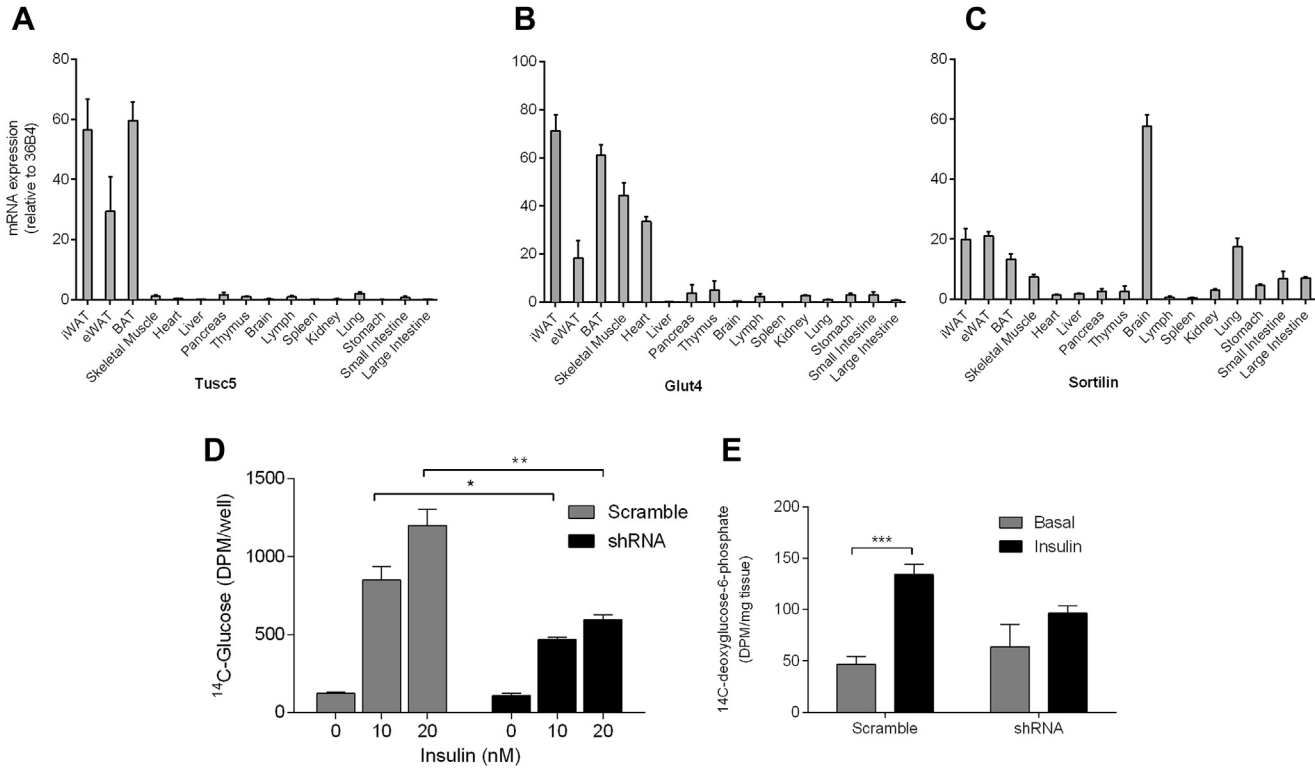


**Figure 1: TUSC5 is adipocyte specifically expressed and is important for insulin-stimulated glucose uptake. (A–C)** qRT-PCR for Tusc5 (A), Glut4 (B) and sortilin (C) mRNA expression in various wild-type C57Bl/6 mouse tissues (n = 5). **(D)** Insulin-stimulated and basal uptake of 2-deoxyglucose in 3T3-L1 adipocytes after shRNA-mediated TUSC5 knockdown (n = 3). **(E)** Insulin-stimulated and basal uptake of 2-deoxyglucose in eWAT of wild-type C57Bl/6 mice 6 days after shRNA-mediated TUSC5 knockdown (n = 6–10).

specific to adipose tissue we first analyzed its role in lipid storage and release. When TUSC5 was ablated in adipocytes (Supplementary Figure 1A and B) basal and insulin-stimulated repression of lipolysis was unaltered (Supplementary Figure 2). Interestingly, TUSC5 knockdown during adipocyte differentiation resulted in smaller lipid droplets (Supplementary Figure 3A and B). As glucose is a key substrate for *de novo* lipogenesis, we investigated whether TUSC5 modulates glucose uptake. Indeed we found that insulin-stimulated glucose uptake in adipocytes was significantly blunted during a TUSC5 knockdown (Figure 1D), while basal glucose uptake was unaffected (Figure 1D).

To confirm these effects *in vivo*, eWAT of wild-type C57Bl/6 mice was injected with adenovirus containing a shRNA targeting TUSC5 (right depot) or a scramble control (left depot), resulting in an approximate 50% ablation of TUSC5 after six days (Supplementary Figure 4A and B). Mice were subsequently tail vein injected with 2-deoxyglucose (in the presence or absence of insulin) and 2-deoxyglucose-6-phosphate (2DOG6P) was precipitated and quantified. Interestingly, we observed a significant difference in glucose uptake between paired depots (i.e. shRNA-eWAT and control-eWAT from the same mouse) only in the TUSC5-ablated eWAT of insulin-stimulated mice (Figure 1E), demonstrating TUSC5's importance in insulin-mediated glucose uptake, *in vivo*. Expression levels of GLUT4 and AKT, as well as phosphorylation of AKT (pAKT), were not affected by TUSC5 knockdown, *in vitro* or *in vivo* (Supplementary Figure 5, data not shown), demonstrating that post-receptor insulin signaling is not dependent on TUSC5.

We next examined the cellular localization of TUSC5 by whole mount staining of eWAT. As shown in Figure 2A, endogenous TUSC5 co-localizes with GLUT4 at the plasma membrane (PM). Since the intracellular area of adipocytes *in vivo* is largely composed of lipids we next examined TUSC5 localization in 3T3-L1 adipocytes. Prior to insulin stimulation TUSC5 is present both intracellularly and at the PM (Figure 2B). Upon insulin stimulation, TUSC5 translocates to the PM, similar to GSVs. Cell fractionation assays confirmed the observed shift of TUSC5 to the PM from the low-density microsome (LDM) vesicle fraction during insulin stimulation (Figure 2C). Further fractionation of the LDM fraction from adipocytes showed that TUSC5 localizes to vesicles of the same density as those containing bona fide GSV proteins such as GLUT4 and sortilin (Supplementary Figure 6). Of note is the fact that Tusc5, in contrast to sortilin and other markers (Figure 1A–C), is only highly expressed in adipose tissue, suggesting that TUSC5 might be the tissue-specific factor connecting GLUT4 with the ubiquitous trafficking machinery.

### 3.2. TUSC5 interacts with GLUT4 and facilitates its membrane fusion

Based upon these observations, we hypothesized that TUSC5 enables vesicle trafficking and/or function. To elucidate its mode of action, we precipitated endogenous TUSC5 and GLUT4 from adipocytes and analyzed co-precipitants by mass spectrometry (MS) using MS1 based label-free quantification (Figure 3A and B and Supplementary Table 1). We could show that endogenous TUSC5 co-precipitates GLUT4 in both a basal and insulin-stimulated state (Figure 3A and B), and vice versa (Figure 4B). Interestingly, a host of proteins known to participate in GLUT4 or GSV trafficking (e.g. IRAP, STX6) [11,15,23] were observed to co-precipitate with both TUSC5 and GLUT4 (Figure 3B). In particular, proteins known to participate in trafficking at the recycling endosome/trans-golgi network (TGN) interface, such as STX16 and VAMP3 [15,18], strongly associate with both proteins (Figure 3B). These data confirm that TUSC5 interacts with the GLUT4 trafficking machinery at various stages of its trafficking cycle.

Since GLUT4 trafficking to the PM is a crucial step for glucose uptake [13], we next investigated GLUT4 exocytosis in response to insulin in the absence of TUSC5. We could show by plasma membrane sheet assay that depletion of TUSC5 did not inhibit insulin-stimulated GLUT4 translocation to the PM (Figure 3C). In fact, in cell fractionation assays, TUSC5 ablation led to an increase of GLUT4 at the PM in a basal state, although no additional increase in GLUT4 presence at the PM was observed after prolonged insulin stimulation (Figure 3D). Thus, TUSC5 ablation does not inhibit glucose uptake by reducing the ability of GLUT4 to traffic to the PM.

As insulin-stimulated GLUT4 translocation remains intact during a TUSC5 knockdown, we investigated GLUT4 membrane fusion using a previously described exofacially myc-tagged GLUT4 construct (GLUT4-myc) [13,46]. Under control conditions transgenic GLUT4-myc is able to fuse with the plasma membrane following insulin stimulation (Figure 3E, left panels) but extracellular myc was not detectable after TUSC5 ablation (Figure 3E, right panels). Similarly, spectrophotometric quantification of extracellular myc-tag exposure confirmed insulin-induced GLUT4-myc membrane fusion inhibition in the absence of TUSC5 (Figure 3F). In all conditions, GLUT4-myc expression remained constant (Supplementary Figure 7). These results demonstrate that the impaired insulin-stimulated glucose uptake observed upon TUSC5 ablation results from a blunting of the GLUT4 fusion mechanism at the PM.

### 3.3. TUSC5 is necessary for proper GLUT4 recycling after insulin stimulation

Based upon our data we hypothesized that TUSC5 participates in GLUT4 recycling after insulin stimulation. To investigate, we performed immunoprecipitation (IP) assays targeting cellugyrin (CG), a protein that marks a distinct non-insulin-responsive GLUT4 vesicle population that is thought to comprise a portion of the endosomal recycling system [49,50] (Supplementary Figure 8). In control cells, IP of CG strongly co-precipitates GLUT4, however this association is severely diminished upon TUSC5 knockdown (Figure 4A). These findings suggest that TUSC5 is a key protein that ensures GLUT4 is able to properly transit through the recycling endosomes.

Since TUSC5 ablation perturbs GLUT4 localization, we hypothesized that the observed glucose uptake phenotype is driven by a reduced association of GLUT4 with key parts of its trafficking machinery. Therefore, we analyzed endogenous GLUT4 co-precipitants by MS in the presence or absence of TUSC5 (Figure 4B). Among others, we identified 10 GLUT4 co-precipitants known to participate in trafficking and analyzed their relative abundances based on their MS1 intensities (Figure 4C). After normalization to GLUT4's average MS1 intensity three proteins, namely IRAP, STX12 and a shared VAMP2/3 peptide, showed a significantly reduced association with GLUT4 in the absence of TUSC5. Further, a reduced association of VAMP2 with GLUT4 on GSVs was confirmed in fractionation assays during a TUSC5 knockdown (Supplementary Figure 9).

To substantiate this, we further investigated the role of TUSC5 in protein recycling. We could show that under control conditions, both VAMP3, an intracellular vesicle fusion protein, and GLUT4 exhibit a predominantly perinuclear localization in a basal state (0 min) and disperse to the plasma membrane after insulin stimulation (15 min) (Figure 4D, E and F). Furthermore, we could show that this initial response is not affected by the knockdown of TUSC5 (Figure 4D, E and F). Interestingly, however, after the engagement of protein recycling during prolonged insulin stimulation (60 and 90 min) only cells expressing TUSC5 still showed a strong membrane staining for GLUT4 and VAMP3 indicating an ability to

properly recycle to the PM, while TUSC5 ablation resulted in aberrant localization of both proteins throughout the intracellular compartment.

Since muscle cells do not express TUSC5, we employed this model to further validate our hypothesis. Therefore, we used L6 cells stably transfected with myc-tagged GLUT4 in the presence or absence of adenoviral mediated TUSC5 overexpression and measured GLUT4 membrane fusion in response to insulin in a time dependent manner. As shown in Figure 4G we observed no changes in basal or insulin-stimulated GLUT4 membrane fusion after 15 min. However, similar

to our results in adipocytes, we observed sustained GLUT4 membrane fusion in cells overexpressing TUSC5 beyond 30 min of insulin stimulation, suggesting that muscle cells, which do not express TUSC5 has different dynamics of glucose uptake compared to TUSC5 expressing adipocytes.

Collectively, these findings demonstrate that TUSC5 is not required for GLUT4 membrane fusion upon an initial insulin stimulus, but rather is necessary for proper protein recycling during prolonged insulin stimulation, a key process in sustained GLUT4 membrane presence and insulin-stimulated glucose uptake.

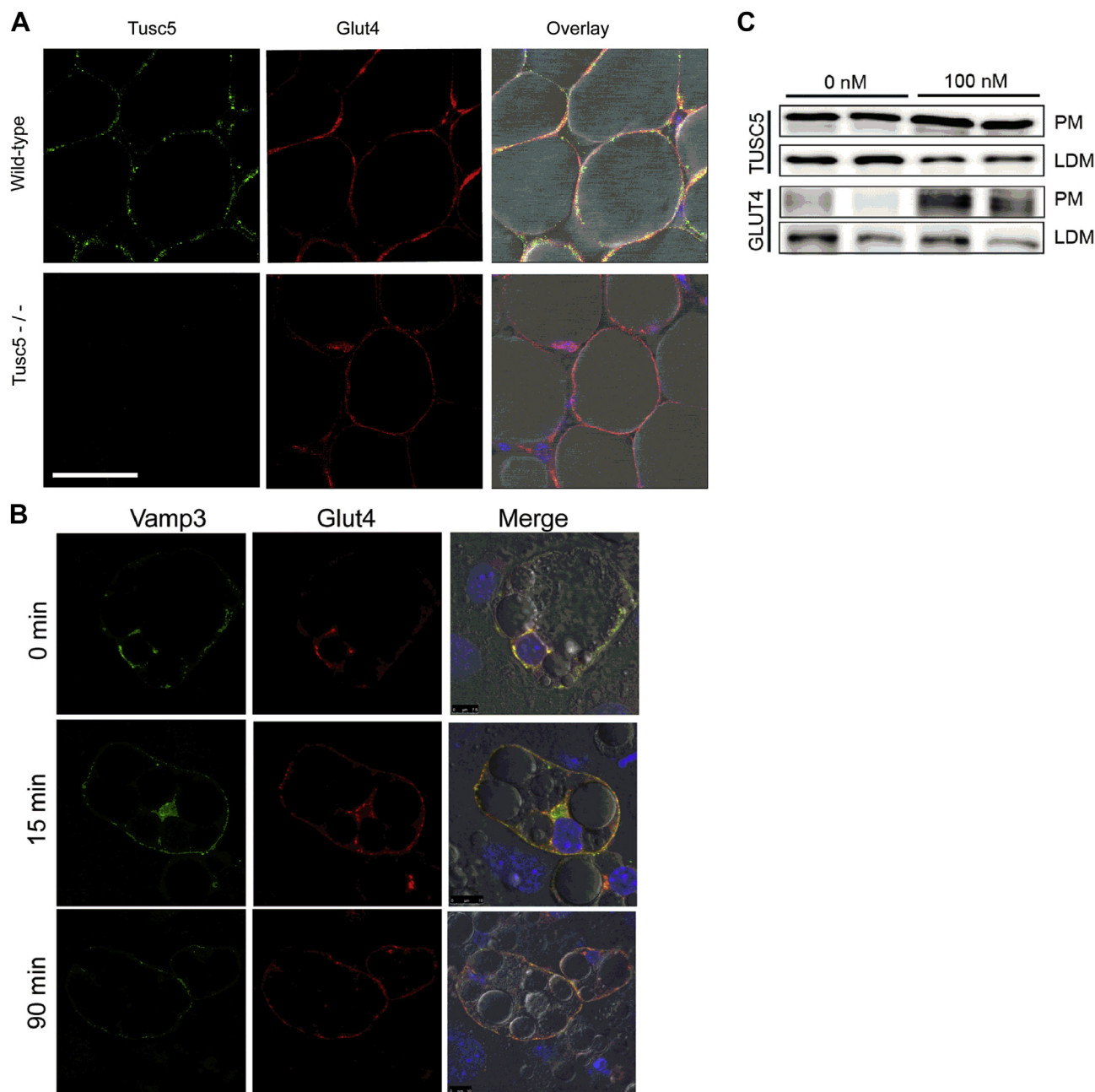


**Figure 2: TUSC5 co-localizes with GLUT4.** (A) Representative immuno-fluorescence images of whole tissue mounts of eWAT from fasted wild-type and *Tusc5* knockout C57Bl/6 mice for TUSC5 and GLUT4 (scale: 100  $\mu$ m). (B) Representative immunofluorescence images of TUSC5 and GLUT4 staining in 3T3-L1 adipocytes in basal (0 nM) and insulin-stimulated state (100 nM) (scale: 50  $\mu$ m) at different time points. (C) Western blot on low-density microsomal (LDM) and plasma membrane fractions from 3T3-L1 adipocytes in basal (0 nM) and insulin-stimulated state (100 nM) for GLUT4 and TUSC5.

### 3.4. TUSC5 ablation leads to hyperglycemia and insulin resistance

To investigate the role of TUSC5 in the development of the metabolic syndrome global *Tusc5* knockout mice were generated. As depicted in Figure 5A, primary adipocytes derived from iWAT, eWAT and BAT from

*Tusc5* knockout mice showed a significantly reduced glucose uptake in response to an insulin stimulus, similar to our cell culture observations, suggesting that TUSC5 might have a function in metabolic homeostasis, *in vivo*. Therefore, to further characterize the role of TUSC5 in

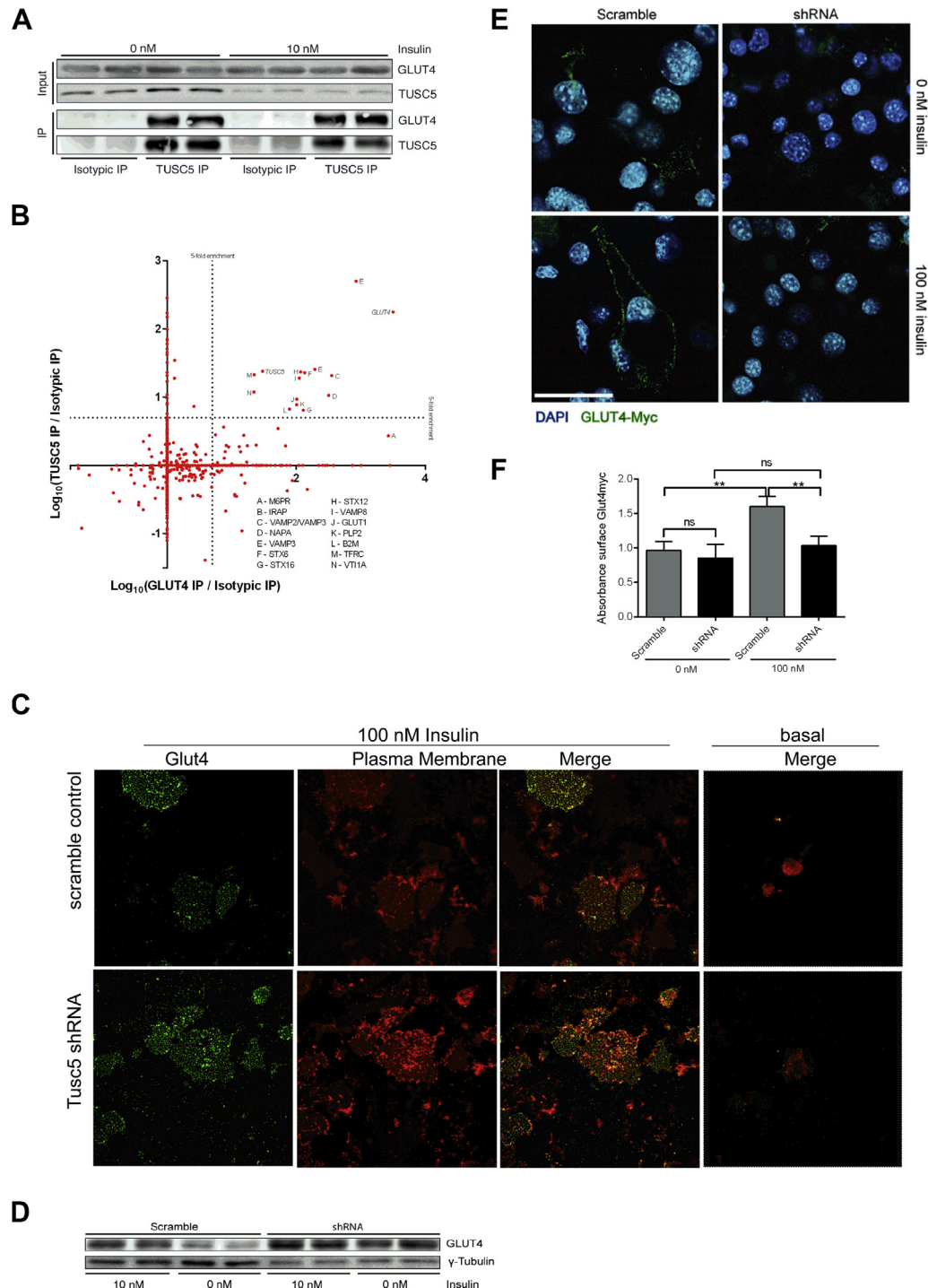


**Figure 3: TUSC5 interacts with GLUT4 and is involved in insulin-stimulated GLUT4 trafficking.** (A) Western blot of immunoprecipitation of endogenous TUSC5 from 3T3-L1 adipocytes in basal (0 nM) and insulin-stimulated state (10 nM). (B) Mass spectrometric identification of co-precipitants from TUSC5 and GLUT4 IPs (n = 4). \**p* < 0.05, \*\**p* < 0.01, \*\*\**p* < 0.001 by Student's *t*-test. Bar graphs shown are mean ± s.e.m. (C) Representative confocal microscopy images of plasma membrane lawns from insulin-stimulated (100 nM, 30 min) 3T3-L1 adipocytes after shRNA-mediated TUSC5 knockdown (scale: 100 μm). (D) Western blot of plasma membrane fractions of 3T3-L1 adipocytes in basal (0 nM) and insulin-stimulated state (10 nM, 2 h) after shRNA-mediated TUSC5 knockdown. (E) Representative confocal microscopy images of non-permeabilized 3T3-L1 adipocytes expressing exofacially myc-tagged GLUT4 after shRNA-mediated TUSC5 knockdown in a basal (0 nM) or insulin-stimulated state (100 nM, 15 min, scale: 100 μm). (F) Quantification of spectrophotometric signal from extracellular myc exposure in basal (0 nM) or insulin-stimulated (100 nM) 3T3-L1 adipocytes.

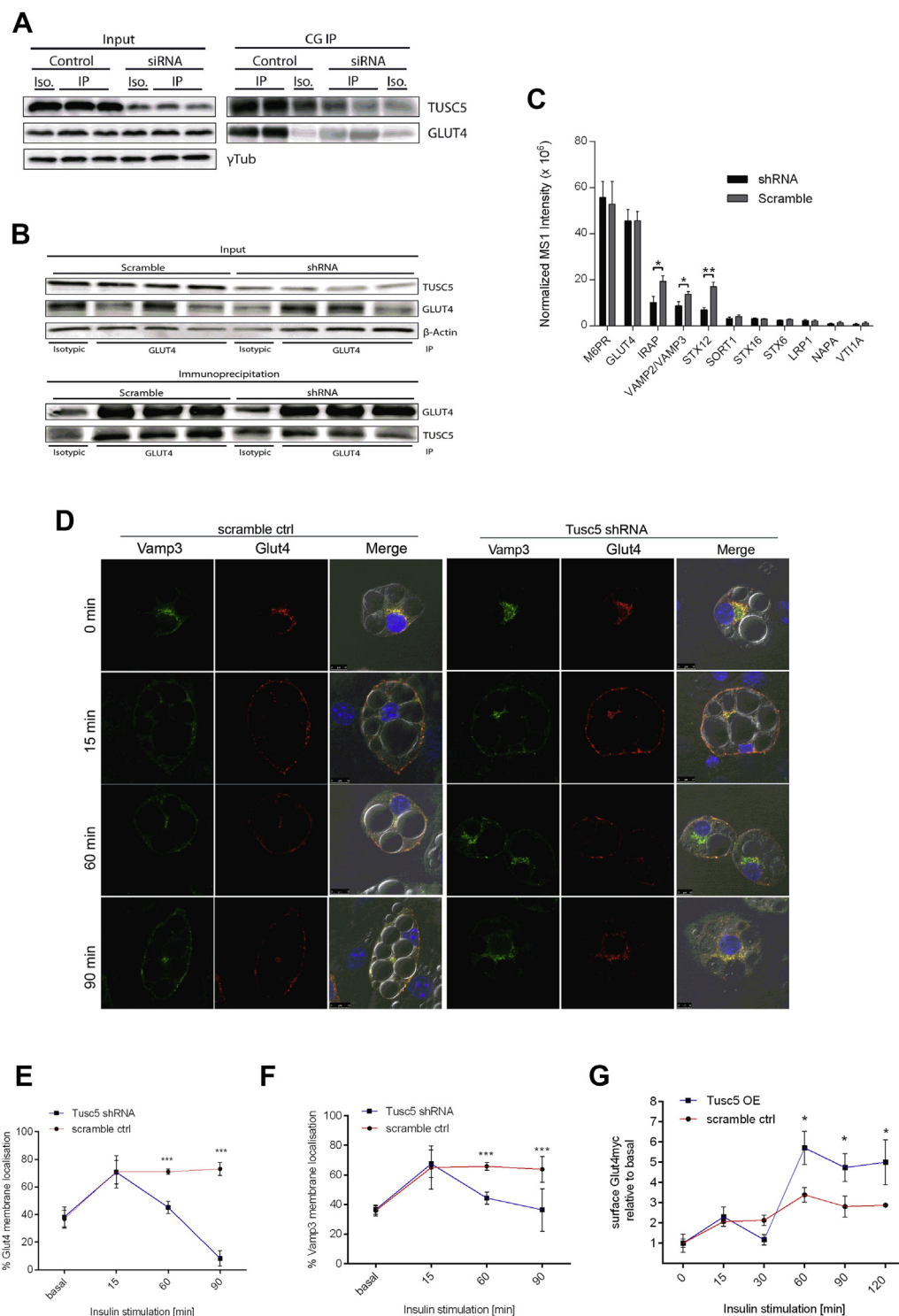


**Figure 4: TUSC5 promotes intracellular associations during protein recycling.** (A) Western blot of immunoprecipitation of endogenous cellugyrin (CG) from 3T3-L1 adipocytes after siRNA-mediated TUSC5 knockdown. (B) Western blot of immunoprecipitation of endogenous GLUT4 from 3T3-L1 adipocytes in control and TUSC5 knockdown conditions. (C) MS1 intensities from mass spectrometric analysis of co-precipitants of GLUT4 IPs as in 2D (n = 4). \* $p < 0.05$ , \*\* $p < 0.01$  by Student's *t*-test. Bar graphs shown are mean  $\pm$  s.e.m. (D) Representative confocal microscopy images of insulin-stimulated 3T3-L1 adipocytes (0, 15, 60 and 90 min stimulation after starvation) after siRNA-mediated TUSC5 knockdown. Quantification of (E) VAMP3 and (F) GLUT4 signal intensities at the plasma membrane from representative confocal microscopy images as shown in 4D. (G) Amount of surface exposed Glut4myc at the indicated time points in basal and insulin-stimulated L6 and L6Glut4myc cells after adenoviral mediated TUSC5 overexpression. \* $p < 0.05$  T5 OE vs. scr ctrl by Student's *t*-test.

metabolic control, *Tusc5* knockout mice were placed on high-fat diet (HFD) along with wild-type littermates. *Tusc5* knockout mice showed complete ablation of TUSC5 expression in iWAT, eWAT and BAT (Supplementary Figure 10) while expression of GLUT4 and other key proteins remained unaltered. On chow diet *Tusc5* knockout mice did not differ from wild-type littermates with respect to weight and glucose clearance (Supplementary Figure 11, data not shown). However, when challenged with a HFD, *Tusc5* knockout mice exhibited a trend towards increased weight gain (Figure 5B). The fat pad weights and total body adiposity, however, did not differ significantly between the two groups (data not shown). Interestingly, *Tusc5* knockout mice exhibited

significantly elevated blood insulin (Figure 5C) and glucose levels (Figure 5D). In line with this, *Tusc5* knockout mice developed insulin resistance as measured by IPGTT and ITT (Figure 5E and F). Taken together, these data demonstrate that TUSC5 is important for glucose disposal and that absence of TUSC5 leads to reduced glucose clearance and the development of insulin resistance.

### 3.5. TUSC5 is a PPAR $\gamma$ target gene conferring the promotion of glucose disposal by PPAR $\gamma$ activators

As TUSC5 is a potential PPAR $\gamma$  target [41] and its expression during 3T3-L1 adipocyte differentiation increases dramatically 1–2 days after

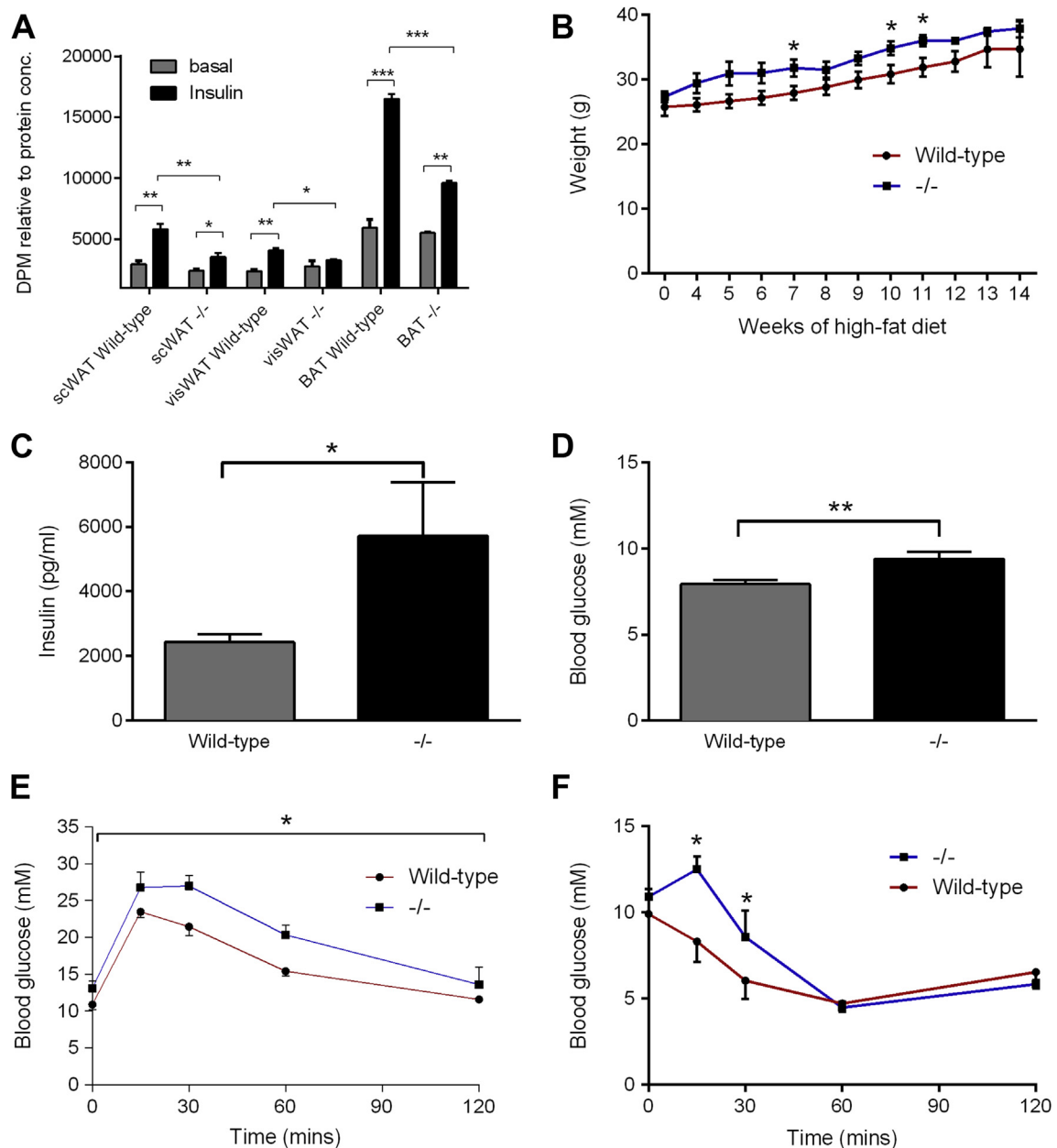


**Figure 5: *Tusc5* knockout mice exhibit impaired blood glucose homeostasis and insulin sensitivity.** (A) *Ex vivo* glucose uptake in white (subcutaneous, visceral) and brown primary adipocytes isolated from wild-type and *Tusc5* knockout mice. (B) Weight of *Tusc5* knockout mice and wild-type littermate controls during HFD feeding (n = 5–6). (C) Re-fed blood glucose and (D) insulin levels in *Tusc5* knockout mice and wild-type littermates after 12 weeks of HFD (n = 5–6). (E) IPGTT (1 g per kg) in *Tusc5* knockout mice and wild-type littermates after 12 weeks of HFD (n = 5–6). (F) ITT (1 IU per kg) in *Tusc5* knockout mice and wild-type littermates after 12 weeks of HFD (n = 3). \**p* < 0.05, \*\**p* < 0.01, \*\*\**p* < 0.001 by Student's *t*-test. Bar graphs shown are mean  $\pm$  s.e.m.

PPAR $\gamma$  induction (Supplementary Figure 12A and B), we next investigated whether TUSC5 is a bona fide PPAR $\gamma$  target gene. To this end, TUSC5 protein levels were examined in mature adipocytes treated with the PPAR $\gamma$  agonist rosiglitazone. TUSC5 protein levels increased during rosiglitazone treatment, peaking at 36–48 h (Figure 6A). Conversely, TUSC5 protein levels were diminished in differentiated brown adipocytes when PPAR $\gamma$  was ablated by siRNA mediated knockdown (Figure 6B). Based on these cell culture findings, we next investigated if TUSC5 is a PPAR $\gamma$  target *in vivo*. C57Bl/6 mice were treated with

rosiglitazone or vehicle orally for 2 weeks and TUSC5 protein levels were examined in iWAT (Figure 6C and D). Rosiglitazone-treated mice showed an 8-fold increase in TUSC5 levels (Figure 6C and D), similar to the increase observed for aP2 and LPL, two known PPAR $\gamma$  target genes.

Based upon these findings, we hypothesized that TUSC5 may confer some of the anti-diabetic effects of PPAR $\gamma$  agonists used in the treatment of type 2 diabetes. To investigate this, *Tusc5* knockout mice and wild-type littermates were placed on a high-fat diet (HFD) to

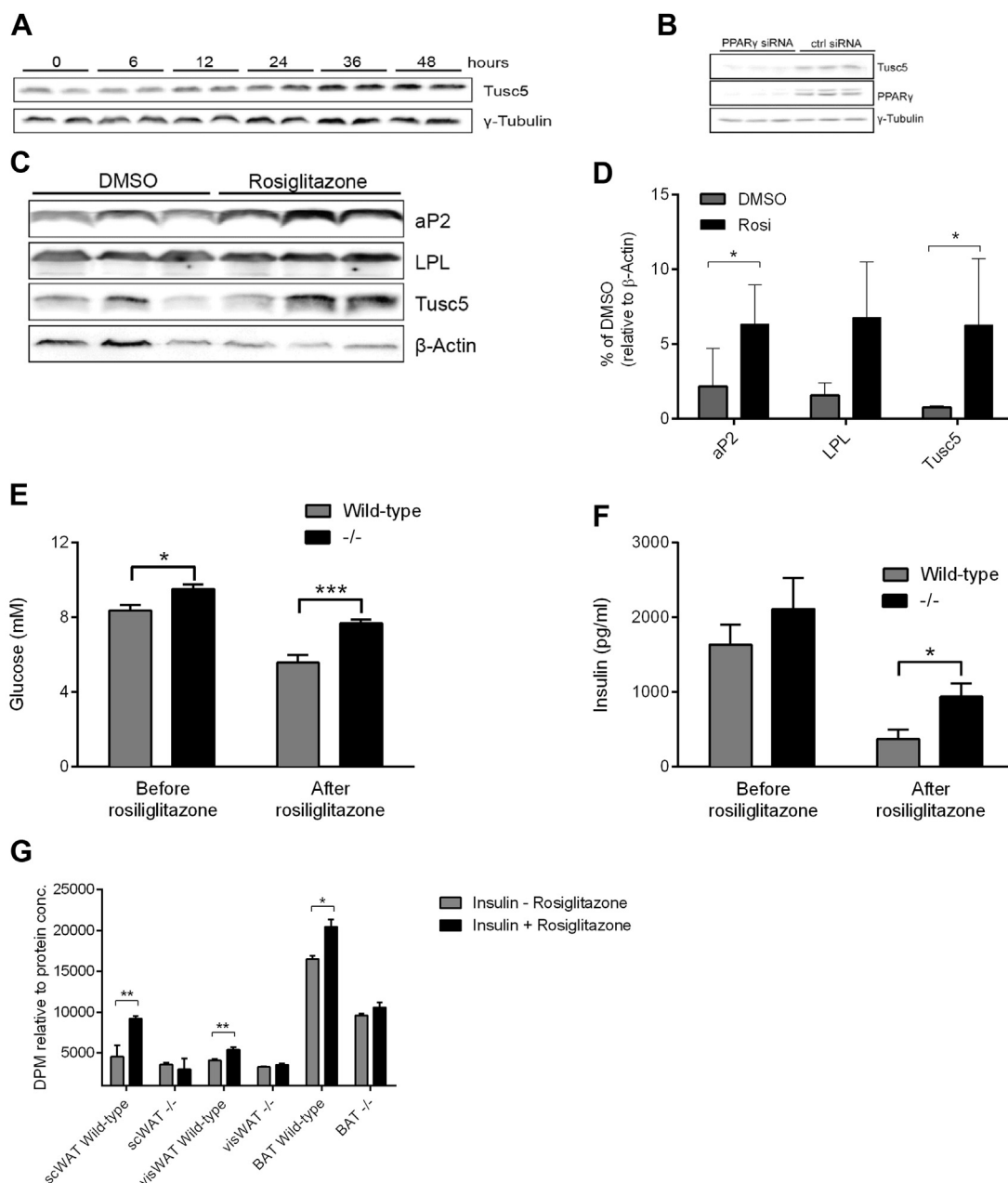


**Figure 6: TUSC5 is target protein of PPAR $\gamma$  and confers the action of TZDs on metabolic health.** (A) Western blot of 3T3-L1 adipocytes stimulated with rosiglitazone (1  $\mu$ M) for indicated times. (B) Western blot of differentiated immortalized brown adipocytes with siRNA mediated PPAR $\gamma$  knockdown. (C) Western blot of iWAT from wild-type C57Bl/6 mice gavaged daily with rosiglitazone (10 mg per kg) for two weeks. (D) Quantification of western blot bands from 5C. (E, F) Fasted blood glucose (E) and insulin (F) levels in *Tusc5* knockout mice and wild-type littermates before and after two weeks of daily rosiglitazone gavage (10 mg per kg) ( $n = 5-6$ ). (G) *Ex vivo* glucose uptake in primary white (subcutaneous/visceral) and brown adipocytes with or without rosiglitazone treatment in basal and insulin-stimulated (100 nM) conditions. \* $p < 0.05$ , \*\* $p < 0.01$  by Student's *t*-test. Bar graphs shown are mean  $\pm$  s.e.m.

induce insulin resistance, at which time the mice were treated orally with rosiglitazone for two weeks. Rosiglitazone treatment significantly reduced both fasting blood glucose (33.3%) and fasting insulin levels (75%) in wild-type mice (Figure 6E and F), but this effect was significantly blunted in *Tusc5* knockout mice (19% reduction in blood glucose and 55% reduction in blood insulin levels).

To substantiate our data, we isolated primary white and brown adipocytes from *Tusc5* knockout and wild-type mice and treated those cells with rosiglitazone. As shown in Figure 6G we observed improved insulin-mediated glucose uptake in cells isolated from wild-type mice treated with rosiglitazone, an effect that was completely abolished in *Tusc5* knockout mice (Figure 6G). Together, these data demonstrate that TUSC5 is a PPAR $\gamma$  target protein that confers some of the beneficial effects of PPAR $\gamma$  activators in the treatment of insulin resistance.

### 3.6. *Tusc5* expression correlates with a healthy metabolic phenotype in humans

Since TUSC5 is important for glucose disposal, *in vitro* and *in vivo*, we next investigated whether *Tusc5* mRNA expression is predictive of the development of insulin resistance in patients. Our first cohort was comprised of lean and obese patients (BMI 20.6 to 38.6). The obese patients were further divided into insulin resistant/type 2 diabetic (according to 2014 ADA criteria of FPG > 7.0 mM and/or 2 h PG > 11.1 mM [51]) and healthy obese patients. Across this entire cohort *Tusc5* mRNA expression in scWAT showed an overall negative correlation with BMI (Figure 7A). However, this correlation significantly diminished when the cohort was stratified based upon their clinical diagnosis. *Tusc5* mRNA expression was only significantly reduced in obese-diabetic patients when compared with lean or obese-healthy patients (Figure 7B), suggesting the correlation observed between *Tusc5* mRNA expression and BMI (Figure 7A) is driven largely by the pathogenesis of type 2 diabetes rather than obesity alone. Supporting this idea is the fact that across the entire cohort *Tusc5* mRNA expression strongly correlates with reduced fasting glucose levels (Figure 7C) and the M-index of insulin resistance as measured by clamp (Figure 7D). To substantiate our hypothesis, we next investigated *Tusc5* mRNA expression in scWAT of a second cohort of exclusively obese individuals (BMIs = 33.6 to 63.7) with varying degrees of insulin sensitivity [52–54]. In this cohort we did not observe a correlation between *Tusc5* mRNA expression in scWAT and BMI (Supplementary Figure 13). However, in agreement with our first patient cohort, *Tusc5* mRNA expression significantly correlated with increased glucose tolerance (Figure 7E) and lower fasting insulin levels (Figure 7F). Collectively, these data show that in patients, *Tusc5* mRNA expression is strongly associated with a healthy metabolic phenotype and that this association is largely independent of BMI.

## 4. DISCUSSION

Although the role of adipose tissue in glucose disposal and the maintenance of metabolic health are well established, many factors that promote glucose clearance remain poorly defined. Our data show for the first time that TUSC5 plays an important *in vivo* function in insulin-stimulated glucose uptake in adipose tissue by affecting proper GLUT4 recycling in response to a prolonged insulin stimulus. Furthermore, we demonstrate that in patients TUSC5 expression correlates with improved insulin sensitivity. Also, the insulin sensitizing effect of the thiazolidinedione (TZD) class of drugs seems to be mediated by TUSC5 to a certain degree.

Insulin-stimulated glucose clearance into adipose tissue ultimately depends on functional GLUT4, which relies on several additional broadly expressed proteins [13,18,19,32,37,55] that predominantly co-localize to the same insulin-responsive vesicles as GLUT4 (GSVs) [21,26,56]. In contrast to other studied GSV proteins, which are expressed in similar vesicle trafficking systems in other tissues [1,21,24–26,57], we show that TUSC5 is the first tissue-specific insulin-responsive protein involved in this process. Based on our data, it is plausible that TUSC5 enables GLUT4 function by utilizing this more ubiquitous system of proteins. This is in line with other tissue-specific proteins for which it has been estimated that roughly half of such proteins interact with more broadly expressed proteins to facilitate their function [58]. In this sense TUSC5 may differentiate insulin-stimulated glucose uptake in adipose tissue and muscle. Based on our data, one could envision a scenario where TUSC5 boosts long-term GLUT4 recycling in adipose tissue, promoting glucose uptake beyond the 30 min post-ingestion peak observed in muscle [59]. Prolonged glucose uptake fits well with the role of adipose tissue as a long-term energy storage organ but more studies focusing on glucose uptake kinetics will be needed to confirm this hypothesis. Given the fact that *Tusc5* expression was reported in primary somatosensory neurons [41] in humans a function for this protein in the regulation of vesicle formation, might be envisaged as well.

Based upon our findings, we hypothesize that TUSC5 ensures the intracellular protein associations that are crucial to the formation of functional GLUT4 vesicles during protein recycling by facilitating protein–protein interactions. TUSC5 co-precipitants are strongly enriched for proteins widely recognized as markers for the recycling endosome and retrograde trafficking including the transferrin receptor [21,27] and the syntaxin 6, syntaxin 16, VAMP3 and Vti1A SNARE bundle [17,60,61]. Moreover, TUSC5 ablation led to disrupted protein distribution during prolonged insulin stimulation, a time frame in which protein recycling is strongly engaged [28,31,55]. This recycling pathway is distinct from, or potentially upstream of, traditional GSV biogenesis from the TGN, a process thought to be driven largely by sortilin [22,37,62,63]. As we hypothesize TUSC5 is functional mainly during insulin-stimulated recycling, our model does not completely preclude the formation of functional GSVs from the TGN (e.g. after protein synthesis or once insulin stimulation is completely removed). In this way, TUSC5 ablation does not halt vesicle formation during protein recycling entirely, but rather impedes correct protein–protein associations. This results in the formation of incomplete vesicles that are depleted of key functional proteins (e.g. VAMP2, VAMP3 and IRAP) and drives the observed vesicle mislocalization and blunted membrane fusion. In fact, specific depletion of these same proteins that show a reduced association with GLUT4 when TUSC5 is ablated (i.e. IRAP and VAMP2/3) recapitulates key elements of our observed TUSC5 knock-down phenotype, including reduced glucose uptake [64,65] and aberrant GLUT4 localization [66,67].

*Tusc5* knockout mice on a high-fat diet exhibit a reduced ability to clear post-prandial glucose but the phenotype observed here is mild when compared to tissue-specific GLUT4 models [4,5]. Interestingly, global *Glut4* knockout mice also exhibit a rather mild metabolic phenotype, a discrepancy attributed to compensatory up-regulation of other glucose transporter protein levels [68], although no such compensation could be detected in *Tusc5* knockout mouse adipose tissue. A key difference between these models and ours is that TUSC5 ablation leaves an abundance of GLUT4 that may retain a degree of function via undisturbed trafficking (i.e. exocytosis from TGN-sourced GSVs), a process that TUSC5 ablation does not preclude. It will be

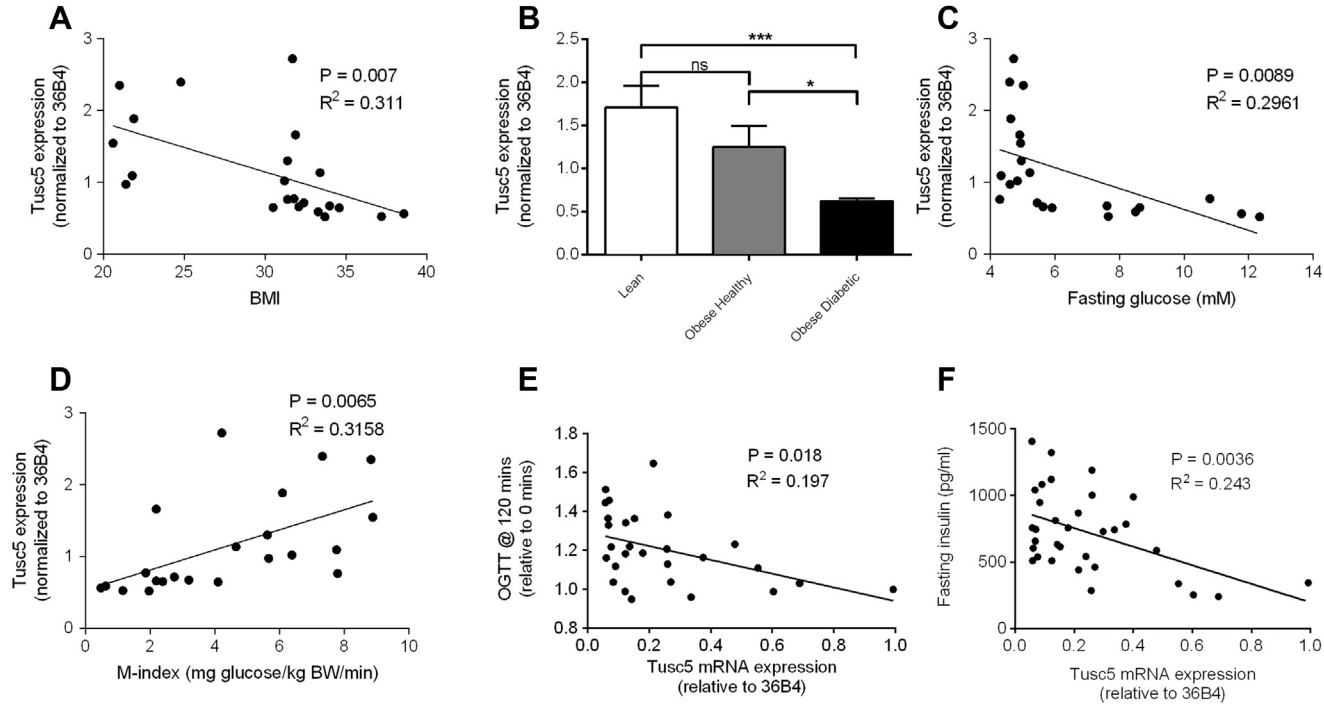


**Figure 7: Tusc5 mRNA expression correlates with retained insulin sensitivity in humans.** (A) qRT-PCR for Tusc5 expression in scWAT biopsies plotted against male patient BMI ( $n = 22$ ). (B) Tusc5 expression in patients from 7A grouped based upon metabolic phenotype (lean ( $n = 6$ ), obese healthy ( $n = 8$ ) or obese diabetic ( $n = 8$ )). (C) Tusc5 expression plotted against fasting glucose in patients from 7A. (D) Tusc5 expression plotted against M-index in patients from 7A. (E–F) qRT-PCR for Tusc5 expression in the adipocyte fraction of scWAT biopsies from a cohort of obese female patients ( $BMI \geq 35$ ) plotted against (E) oral glucose tolerance (OGTT) at 2 h and (F) fasting insulin ( $n = 33$ ).  $*p < 0.05$ ,  $***p < 0.001$  by Student's *t*-test. Bar graphs shown are mean  $\pm$  s.e.m. Graphs A, C, D, E, and F analyzed by linear regression.

important to investigate the degree to which this trafficking route exists in *Tusc5* knockout mice and can compensate for disrupted recycling. Many pharmaceutical treatments (i.e. TZDs) improve insulin sensitivity in type 2 diabetics by selectively agonizing the nuclear transcription factor PPAR $\gamma$  [69]. However, the mechanism of action of these drugs is incompletely understood. Our data confirm TUSC5 as a PPAR $\gamma$  target *in vitro* and *in vivo* and further demonstrate, in accordance with previous work, that the insulin sensitizing effect of rosiglitazone is mediated in part by through TUSC5 [57]. A past study found no increase in *Tusc5* mRNA in pioglitazone-treated patients. However, due to the small cohort size, it remains unclear whether *Tusc5* is regulated in response to TZDs in patients. Our finding is particularly interesting as it may open new avenues for the treatment of type 2 diabetes with potentially less pronounced side effects, especially if TUSC5 levels or function can be manipulated pharmaceutically. Further, our patient data support the importance of TUSC5 in the face of obesity as two cohorts show that TUSC5 levels are predictive of improved insulin sensitivity. This finding may provide an explanation as to why a sub-set of individuals manage to stave off insulin resistance and type 2 diabetes despite chronic obesity [70,71].

In conclusion, our present study identifies TUSC5 as a novel regulator of prolonged insulin stimulated GLUT4 trafficking, thereby regulating glucose uptake in adipocytes. Furthermore, our studies qualify TUSC5 as a unique insulin-responsive protein conferring tissue specificity to the GLUT4 translocation machinery via the promotion of proper protein recycling. As glucose disposal via GLUT4 is integral to the maintenance of insulin sensitivity and the prevention of diabetes during obesity, TUSC5 may be critical in the progression of this disease [4,5]. Given the fact that TUSC5 regulates vesicle fusion and recycling it is at the moment difficult to envisage how this protein could be targeted to improve glucose homeostasis. Future studies on TUSC5 may bring a deeper understanding of GLUT4 and its role in the maintenance of glucose homeostasis in obesity.

## ACKNOWLEDGMENTS

We wish to thank M. Geiger, E. Weber, A. Mitkova, M. Balaz, M. Vlcek and T. Kurdiová for technical help. Thanks to A. Klip, P. Bilan and K. Foley for their help with GLUT4-myc experimental design. We also wish to thank G. Grandl, M. Rosenwald, E. Luca and M. Stoffel for manuscript revision and discussions. The work was supported by the ERC (CW) the SNF (CW) and the Thyssen Foundation (CW).

## CONFLICT OF INTEREST

None declared.

## APPENDIX A. SUPPLEMENTARY DATA

Supplementary data related to this article can be found at <http://dx.doi.org/10.1016/j.molmet.2015.08.003>.

## REFERENCES

- [1] Huang, S., Czech, M.P., 2007. The GLUT4 glucose transporter. *Cell Metabolism* 5:237–252.
- [2] Maier, V.H., Gould, G.W., 2000. Long-term insulin treatment of 3T3-L1 adipocytes results in mis-targeting of GLUT4: implications for insulin-stimulated glucose transport. *Diabetologia* 43:1273–1281.
- [3] Garvey, W.T., Maianu, L., Zhu, J.H., Brechtel-Hook, G., Wallace, P., Baron, A.D., 1998. Evidence for defects in the trafficking and translocation of GLUT4 glucose transporters in skeletal muscle as a cause of human insulin resistance. *Journal of Clinical Investigation* 101:2377–2386.
- [4] Zisman, A., Peroni, O., Abel, E., Michael, M., Mauvais-Jarvis, F., Lowell, B., et al., 2000. Targeted disruption of the glucose transporter 4 selectively in muscle causes insulin resistance and glucose intolerance. *Nature Medicine* 6: 924–928.
- [5] Abel, E.D., Peroni, O., Kim, J.K., Kim, Y.B., Boss, O., Hadro, E., et al., 2001. Adipose-selective targeting of the GLUT4 gene impairs insulin action in muscle and liver. *Nature* 409:729–733.
- [6] Stenbit, A.E., Tsao, T.S., Li, J., Burcelin, R., Geenen, D.L., Factor, S.M., et al., 1997. GLUT4 heterozygous knockout mice develop muscle insulin resistance and diabetes. *Nature Medicine* 3:1096–1101.
- [7] Carvalho, E., 2005. Adipose-specific overexpression of GLUT4 reverses insulin resistance and diabetes in mice lacking GLUT4 selectively in muscle. *AJP: Endocrinology and Metabolism* 289:E551–E561.
- [8] Tozzo, E., Gnudi, L., Kahn, B.B., 1997. Amelioration of insulin resistance in streptozotocin diabetic mice by transgenic overexpression of GLUT4 driven by an adipose-specific promoter. *Endocrinology* 138:1604–1611.
- [9] Leturque, A., Loizeau, M., Vaulont, S., Salminen, M., Girard, J., 1996. Improvement of insulin action in diabetic transgenic mice selectively overexpressing GLUT4 in skeletal muscle. *Diabetes* 45:23–27.
- [10] Ren, J.M., Marshall, B.A., Mueckler, M.M., McCaleb, M., Amatruda, J.M., Shulman, G.I., 1995. Overexpression of Glut4 protein in muscle increases basal and insulin-stimulated whole body glucose disposal in conscious mice. *Journal of Clinical Investigation* 95:429–432.
- [11] Leto, D., Saltiel, A.R., 2012. Regulation of glucose transport by insulin: traffic control of GLUT4. *Nature Reviews Molecular Cell Biology* 13:383–396.
- [12] Bogan, J.S., 2012. Regulation of glucose transporter translocation in health and diabetes. *Annual Review of Biochemistry* 81:507–532.
- [13] Kanai, F., Nishioka, Y., Hayashi, H., Kamohara, S., Todaka, M., Ebina, Y., 1993. Direct demonstration of insulin-induced GLUT4 translocation to the surface of intact cells by insertion of a c-myc epitope into an exofacial GLUT4 domain. *Journal of Biological Chemistry* 268:14523–14526.
- [14] Randhawa, V.K., Bilan, P.J., Khayat, Z.A., Daneman, N., Liu, Z., Ramlal, T., et al., 2000. VAMP2, but not VAMP3/cellubrevin, mediates insulin-dependent incorporation of GLUT4 into the plasma membrane of L6 myoblasts. *Molecular Biology of the Cell* 11:2403–2417.
- [15] Bryant, N.J., Gould, G.W., 2011. SNARE proteins underpin insulin-regulated GLUT4 traffic. *Traffic* 12:657–664.
- [16] Keller, S.R., Scott, H.M., Mastick, C.C., Aebersold, R., Lienhard, G.E., 1995. Cloning and characterization of a novel insulin-regulated membrane aminopeptidase from Glut4 vesicles. *Journal of Biological Chemistry* 270:23612–23618.
- [17] Perera, H.K.I., Clarke, M., Morris, N.J., Hong, W., Chamberlain, L.H., Gould, G.W., 2003. Syntaxin 6 regulates Glut4 trafficking in 3T3-L1 adipocytes. *Molecular Biology of the Cell* 14:2946–2958.
- [18] Shewan, A.M., van Dam, E.M., Martin, S., Luen, T.B., Hong, W., Bryant, N.J., et al., 2003. GLUT4 recycles via a trans-Golgi network (TGN) subdomain enriched in syntaxins 6 and 16 but not TGN38: involvement of an acidic targeting motif. *Molecular Biology of the Cell* 14:973–986.
- [19] Bogan, J.S., Hendon, N., McKee, A.E., Tsao, T.-S., Lodish, H.F., 2003. Functional cloning of TUG as a regulator of GLUT4 glucose transporter trafficking. *Nature* 425:727–733.
- [20] Sano, H., 2003. Insulin-stimulated phosphorylation of a Rab GTPase-activating protein regulates GLUT4 translocation. *Journal of Biological Chemistry* 278: 14599–14602.
- [21] Jedrychowski, M.P., Gartner, C.A., Gygi, S.P., Zhou, L., Herz, J., Kandror, K.V., et al., 2010. Proteomic analysis of GLUT4 storage vesicles reveals LRP1 to be an important vesicle component and target of insulin signaling. *Journal of Biological Chemistry* 285:104–114.

- [22] Pilch, P.F., 2007. The mass action hypothesis: formation of Glut4 storage vesicles, a tissue-specific, regulated exocytic compartment. *Acta Physiologica* 192:89–101.
- [23] Kandror, K.V., Pilch, P.F., 2011. The sugar is sIRVed: sorting Glut4 and its fellow travelers. *Traffic* 12:665–671.
- [24] Barile, M., 2005. Large scale protein identification in intracellular aquaporin-2 vesicles from renal inner medullary collecting duct. *Molecular & Cellular Proteomics* 4:1095–1106.
- [25] Burré, J., Beckhaus, T., Schägger, H., Corvey, C., Hofmann, S., Karas, M., et al., 2006. Analysis of the synaptic vesicle proteome using three gel-based protein separation techniques. *Proteomics* 6:6250–6262.
- [26] Brunner, Y., Coute, Y., Iezzi, M., Foti, M., Fukuda, M., Hochstrasser, D.F., et al., 2007. Proteomics analysis of insulin secretory granules. *Molecular & Cellular Proteomics* 6:1007–1017.
- [27] Foley, K., Boguslavsky, S., Klip, A., 2011. Endocytosis, recycling, and regulated exocytosis of glucose transporter 4. *Biochemistry* 50:3048–3061.
- [28] Muretta, J.M., Romenskaia, I., Mastick, C.C., 2007. Insulin releases Glut4 from static storage compartments into cycling endosomes and increases the rate constant for Glut4 exocytosis. *Journal of Biological Chemistry* 283:311–323.
- [29] Blot, V., McGraw, T.E., 2006. GLUT4 is internalized by a cholesterol-dependent nystatin-sensitive mechanism inhibited by insulin. *EMBO Journal* 25:5648–5658.
- [30] Shigematsu, S., 2003. The adipocyte plasma membrane caveolin functional/structural organization is necessary for the efficient endocytosis of GLUT4. *Journal of Biological Chemistry* 278:10683–10690.
- [31] Govers, R., Coster, A.C.F., James, D.E., 2004. Insulin increases cell surface GLUT4 levels by dose dependently discharging GLUT4 into a cell surface recycling pathway. *Molecular Cell Biology* 24:6456–6466.
- [32] Mallard, F., 2002. Early/recycling endosomes-to-TGN transport involves two SNARE complexes and a Rab6 isoform. *Journal of Cell Biology* 156:653–664.
- [33] Millar, C.A., Shewan, A., Hickson, G.R., James, D.E., Gould, G.W., 1999. Differential regulation of secretory compartments containing the insulin-responsive glucose transporter 4 in 3T3-L1 adipocytes. *Molecular Biology of the Cell* 10:3675–3688.
- [34] Lampson, M.A., Racz, A., Cushman, S.W., McGraw, T.E., 2000. Demonstration of insulin-responsive trafficking of GLUT4 and vPTR in fibroblasts. *Journal of Cell Science* 113(Pt 22):4065–4076.
- [35] Ramm, G., Slot, J.W., James, D.E., Stoorvogel, W., 2000. Insulin recruits GLUT4 from specialized VAMP2-carrying vesicles as well as from the dynamic endosomal/trans-Golgi network in rat adipocytes. *Molecular Biology of the Cell* 11:4079–4091.
- [36] Blot, V., McGraw, T.E., 2008. Molecular mechanisms controlling GLUT4 intracellular retention. *Molecular Biology of the Cell* 19:3477–3487.
- [37] Shi, J., Huang, G., Kandror, K.V., 2008. Self-assembly of Glut4 storage vesicles during differentiation of 3T3-L1 adipocytes. *Journal of Biological Chemistry* 283:30311–30321.
- [38] Shibata, T., Koide, H., Hayashi, R., Nagata, K., Takeo, C., Yoshida, T., et al., 2007. Molecular cloning and characterization of rat brain endothelial cell derived gene-1 (tumor suppressor candidate 5) expressing abundantly in adipose tissues. *Molecular and Cellular Endocrinology* 263:38–45.
- [39] Koide, H., Shibata, T., Yamada, N., Asaki, T., Nagao, T., Yoshida, T., et al., 2007. Tumor suppressor candidate 5 (TUSC5) is expressed in brown adipocytes. *Biochemical and Biophysical Research Communications* 360:139–145.
- [40] Oort, P.J., Warden, C.H., Baumann, T.K., Knotts, T.A., Adams, S.H., 2007. Characterization of Tusc5, an adipocyte gene co-expressed in peripheral neurons. *Molecular and Cellular Endocrinology* 276:24–35.
- [41] Knotts, T.A., Lee, H.W., Kim, J.B., Oort, P.J., Mcpherson, R., Dent, R., et al., 2009. Molecular characterization of the tumor suppressor candidate 5 gene: regulation by PPAR $\gamma$  and identification of TUSC5 coding variants in lean and obese humans. *PPAR Research* 2009:1–14.
- [42] Meissburger, B., Ukropec, J., Roeder, E., Beaton, N., Geiger, M., Teupser, D., et al., 2011. Adipogenesis and insulin sensitivity in obesity are regulated by retinoid-related orphan receptor gamma. *EMBO Molecular Medicine* 3:637–651.
- [43] Mrosek, N., Meissburger, B., Matak, C., Roeder, E., Ukropec, J., Klimes, I., et al., 2013. Transcriptional regulation of adipocyte formation by the liver receptor homologue 1 (Lrh1)-Small hetero-dimerization partner (Shp) network. *Molecular Metabolism* 2:314–323.
- [44] Elmendorf, J.S., Boeglin, D.J., Pessin, J.E., 1999. Temporal separation of insulin-stimulated GLUT4/IRAP vesicle plasma membrane docking and fusion in 3T3L1 adipocytes. *The Journal of Biological Chemistry* 274:37357–37361.
- [45] Joost, H.G., Schürmann, A., 2001. Subcellular fractionation of adipocytes and 3T3-L1 cells. *Methods in Molecular Biology* 155:77–82.
- [46] Wang, Q., Khayat, Z., Kishi, K., Ebina, Y., Klip, A., 1998. GLUT4 translocation by insulin in intact muscle cells: detection by a fast and quantitative assay. *FEBS Letters* 427:193–197.
- [47] Antonescu, C.N., Díaz, M., Femia, G., Planas, J.V., Klip, A., 2008. Clathrin-dependent and independent endocytosis of glucose transporter 4 (GLUT4) in myoblasts: regulation by mitochondrial uncoupling. *Traffic* 9:1173–1190.
- [48] Ukropec, J., Penesová, A., Škopková, M., Pura, M., Vlíček, M., Rádková, Ž., et al., 2008. Adipokine protein expression pattern in growth hormone deficiency predisposes to the increased fat cell size and the whole body metabolic derangements. *The Journal of Clinical Endocrinology and Metabolism* 93:2255–2262.
- [49] Kupriyanova, T.A., 2002. Isolation and characterization of the two major intracellular Glut4 storage compartments. *Journal of Biological Chemistry* 277:9133–9138.
- [50] Kupriyanova, T.A., 2000. Cellugyrin is a marker for a distinct population of intracellular Glut4-containing vesicles. *Journal of Biological Chemistry* 275:36263–36268.
- [51] Association A.D., 2014. Standards of medical care in diabetes—2014. *Diabetes Care* 37(Suppl 1):S14–S80.
- [52] Challa, T.D., Beaton, N., Arnold, M., Rudofsky, G., Langhans, W., Wolfrum, C., 2012. Regulation of adipocyte formation by GLP-1/GLP-1R signaling. *Journal of Biological Chemistry* 287:6421–6430.
- [53] Rohm, M., Sommerfeld, A., Strzoda, D., Jones, A., Sijmonsma, T.P., Rudofsky, G., et al., 2013. Transcriptional cofactor TBLR1 controls lipid mobilization in white adipose tissue. *Cell Metabolism* 17:575–585.
- [54] Rudofsky, G., Roeder, E., Merle, T., Hildebrand, M., Nawroth, P.P., Wolfrum, C., 2011. Weight loss improves endothelial function independently of ADMA reduction in severe obesity. *Hormone and Metabolic Research* 43:343–348.
- [55] Xu, Y., Rubin, B.R., Orme, C.M., Karpikov, A., Yu, C., Bogan, J.S., et al., 2011. Dual-mode of insulin action controls GLUT4 vesicle exocytosis. *The Journal of Cell Biology* 193:643–653.
- [56] Song, X., Lichti, C.F., Townsend, R.R., Mueckler, M., 2013. Single Point mutations result in the miss-sorting of Glut4 to a novel membrane compartment associated with stress granule proteins. *PLoS One* 8:e68516.
- [57] Fazakerley, D.J., Naghilo, S., Chaudhuri, R., Koumanov, F., Burchfield, J.G., Thomas, K.C., et al., 2015. Proteomic analysis of GLUT4 storage vesicles reveals tumour suppressor candidate 5 (TUSC5) as a novel regulator of insulin action in adipocytes. *Journal of Biological Chemistry* [published online].
- [58] Bossi, A., Lehner, B., 2009. Tissue specificity and the human protein interaction network. *Molecular Systems Biology* 5:1–7.
- [59] Kelley, D., Mitrakou, A., Marsh, H., Schwenk, F., Benn, J., Sonnenberg, G., et al., 1988. Skeletal muscle glycolysis, oxidation, and storage of an oral glucose load. *Journal of Clinical Investigation* 81:1563–1571.
- [60] Johannes, L., Popoff, V., 2008. Tracing the retrograde route in protein trafficking. *Cell* 135:1175–1187.
- [61] Proctor, K.M., Miller, S.C.M., Bryant, N.J., Gould, G.W., 2006. Syntaxin 16 controls the intracellular sequestration of GLUT4 in 3T3-L1 adipocytes. *Biochemical and Biophysical Research Communications* 347:433–438.
- [62] Shi, J., Kandror, K.V., 2005. Sortilin is essential and sufficient for the formation of Glut4 storage vesicles in 3T3-L1 adipocytes. *Developmental Cell* 9:99–108.

- [63] Shi, J., Kandror, K.V., 2007. The luminal Vps10p domain of sortilin plays the predominant role in targeting to insulin-responsive Glut4-containing vesicles. *Journal of Biological Chemistry* 282:9008–9016.
- [64] Kawaguchi, T., Tamori, Y., Kanda, H., Yoshikawa, M., Tateya, S., Nishino, N., et al., 2010. The t-SNAREs syntaxin4 and SNAP23 but not v-SNARE VAMP2 are indispensable to tether GLUT4 vesicles at the plasma membrane in adipocyte. *Biochemical and Biophysical Research Communications* 391:1336–1341.
- [65] Williams, D., Pessin, J.E., 2008. Mapping of R-SNARE function at distinct intracellular GLUT4 trafficking steps in adipocytes. *The Journal of Cell Biology* 180:375–387.
- [66] Larance, M., Ramm, G., Stöckli, J., van Dam, E.M., Winata, S., Wasinger, V., et al., 2005. Characterization of the role of the Rab GTPase-activating protein AS160 in insulin-regulated GLUT4 trafficking. *Journal of Biological Chemistry* 280:37803–37813.
- [67] Waters, S.B., D'Auria, M., Martin, S.S., Nguyen, C., Kozma, L.M., Luskey, K.L., 1997. The amino terminus of insulin-responsive aminopeptidase causes Glut4 translocation in 3T3-L1 adipocytes. *Journal of Biological Chemistry* 272: 23323–23327.
- [68] Katz, E.B., Stenbit, A.E., Hatton, K., DePinho, R., Charron, M.J., 1995. Cardiac and adipose tissue abnormalities but not diabetes in mice deficient in GLUT4. *Nature* 377:151–155.
- [69] Consoli, A., Formoso, G., 2013. Do thiazolidinediones still have a role in treatment of type 2 diabetes mellitus? *Diabetes, Obesity and Metabolism* 15: 967–977.
- [70] Kahn, S.E., Hull, R.L., Utzschneider, K.M., 2006. Mechanisms linking obesity to insulin resistance and type 2 diabetes. *Nature* 444:840–846.
- [71] Després, J.-P., Lemieux, I., 2006. Abdominal obesity and metabolic syndrome. *Nature* 444:881–887.